Article

Neuron

Direct Ventral Hippocampal-Prefrontal Input Is Required for Anxiety-Related Neural Activity and Behavior

Highlights

- The vHPC-mPFC pathway is required for normal anxiety-like behavior
- Anxiety-related increases in vHPC-mPFC theta synchrony require direct vHPC-mPFC input
- Spatial representations of aversion in the mPFC are dependent on direct vHPC input
- The effects of inhibition of vHPC inputs are task, pathway, and frequency specific

Authors

Nancy Padilla-Coreano, Scott S. Bolkan, Georgia M. Pierce, ..., Alvaro L. Garcia-Garcia, Timothy J. Spellman, Joshua A. Gordon

Correspondence

jg343@columbia.edu

In Brief

Padilla-Coreano et al. use optogenetic inhibition and multi-site neurophysiology to demonstrate pathway- and frequency-specific effects of inhibiting ventral hippocampal input to the medial prefrontal cortex. Terminal inhibition reduced anxiety-like behavior, theta synchrony, and spatial representations of aversion within the cortex.

Padilla-Coreano et al., 2016, Neuron *89*, 857–866
February 17, 2016
http://dx.doi.org/10.1016/j.neuron.2016.01.011

CellPress

Neuron
Article

Direct Ventral Hippocampal-Prefrontal Input Is Required for Anxiety-Related Neural Activity and Behavior

Nancy Padilla-Coreano,[1,2] Scott S. Bolkan,[1,2] Georgia M. Pierce,[1] Dakota R. Blackman,[3] William D. Hardin,[2] Alvaro L. Garcia-Garcia,[2] Timothy J. Spellman,[4] and Joshua A. Gordon[2,5,*]
[1]Department of Neuroscience
[2]Department of Psychiatry
Columbia University, 1051 Riverside Drive, New York, NY 10032, USA
[3]Department of Neuroscience, Barnard College, 3009 Broadway, New York, NY 10027, USA
[4]Department of Physiology and Cellular Biophysics, Columbia University, 622 West 168th Street, New York, NY 10032, USA
[5]Division of Integrative Neuroscience, New York State Psychiatric Institute, 1051 Riverside Drive, New York, NY 10032 USA
*Correspondence: jg343@columbia.edu
http://dx.doi.org/10.1016/j.neuron.2016.01.011

SUMMARY

The ventral hippocampus (vHPC), medial prefrontal cortex (mPFC), and basolateral amygdala (BLA) are each required for the expression of anxiety-like behavior. Yet the role of each individual element of the circuit is unclear. The projection from the vHPC to the mPFC has been implicated in anxiety-related neural synchrony and spatial representations of aversion. The role of this projection was examined using multi-site neural recordings combined with optogenetic terminal inhibition. Inhibition of vHPC input to the mPFC disrupted anxiety and mPFC representations of aversion, and reduced theta synchrony in a pathway-, frequency- and task-specific manner. Moreover, bilateral, but not unilateral, inhibition altered physiological correlates of anxiety in the BLA, mimicking a safety-like state. These results reveal a specific role for the vHPC-mPFC projection in anxiety-related behavior and the spatial representation of aversive information within the mPFC.

INTRODUCTION

Anxiety is usually an adaptive state of increased apprehension that helps an animal avoid potential danger. However, inappropriate expression of anxiety is maladaptive and, in humans, can lead to anxiety disorders. In order to develop better treatments for these disorders, we must understand the neural circuits that support normal anxiety. Studies in rodents have shown that anxiety-like behavior involves the ventral hippocampus (vHPC), medial prefrontal cortex (mPFC), and basolateral amygdala (BLA) (Kjelstrup et al., 2002; Maren and Holt, 2004; Shah and Treit, 2003; Sierra-Mercado et al., 2011; Tye et al., 2011). These three regions share anatomical and functional connectivity (Hoover and Vertes, 2007; Lesting et al., 2011, 2013; Likhtik et al., 2014; Pikkarainen et al., 1999), suggesting they function as a distributed network that supports anxiety behavior in an interdependent manner.

In particular, the direct monosynaptic projection from the vHPC to the mPFC appears to be a key component of this circuit, especially during the expression of innate forms of anxiety-like behavior. In rodents, theta-frequency (4–12 Hz) synchrony emerges between the vHPC and mPFC during exposure to anxiogenic environments such as the elevated plus maze (EPM) (Adhikari et al., 2010). Moreover, single units in the mPFC that are synchronized with vHPC theta preferentially represent armtype in the EPM (Adhikari et al., 2011), suggesting that vHPC input is necessary for this representation.

The high degree of interconnectivity in the vHPC-mPFC-BLA circuit and presence of multiple interacting oscillatory activity patterns complicate the picture. Theta-frequency synchrony between the vHPC-BLA and BLA-mPFC is also enhanced during innate forms of anxiety (Lesting et al., 2011; Likhtik et al., 2014; Stujenske et al., 2014), and optogenetic inhibition of the projection from the BLA to the vHPC is anxiolytic (Felix-Ortiz et al., 2013). While theta power is increased with anxiety, fast gamma power is decreased, both in the BLA and mPFC (Stujenske et al., 2014). Even so, coupling between theta and gamma oscillations within the BLA is enhanced by anxiety (Stujenske et al., 2014). Finally, anxiety state modulates the directionality of oscillatory interactions between the mPFC and BLA, such that relative safety is associated with a shift toward enhanced mPFC influence over the BLA in both theta- and gamma-frequency ranges (Likhtik et al., 2014; Stujenske et al., 2014). These findings emphasize the degree to which each of these three structures functions within an interconnected, interacting circuit.

What then might be the role of an individual element within such an interactive circuit? Is the direct vHPC-to-mPFC pathway required for anxiety-like behavior, or might the indirect pathway through the BLA suffice in its absence? And what information does the direct pathway carry? Here we specifically test the role of the direct projection from the vHPC in the expression of anxiety-like behavior, synchrony within vHPC-mPFC-BLA circuit, and the representation of valence in the EPM. Furthermore,

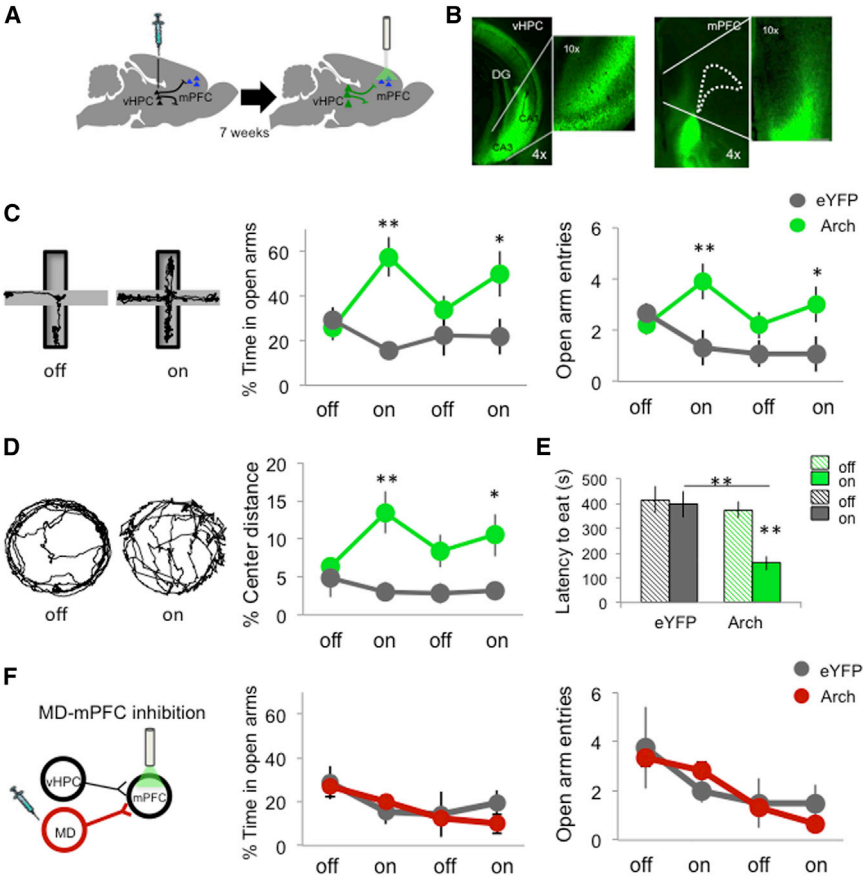

Figure 1. Selective Inhibition of Hippocampal-Prefrontal Input Disrupts Avoidance Behavior

(A) Schematic of viral injection and terminal illumination.

(B) Coronal views of eYFP fluorescence in vHPC somata (left) and terminals within the mPFC (right). Dotted line lines indicate frontal white matter.

(C) Paths for an example mouse during laser off and on in the EPM. Right, Open arm avoidance in vHPC Arch- and eYFP-expressing animals (Arch n = 12; eYFP n = 12; two-way ANOVA, interaction of light and virus, $F_{(1,47)} = 9.15$ $p = 0.0043$; *$p < 0.02$, **$p < 0.005$ for Arch versus eYFP, post hoc Bonferroni-corrected t test).

(D) Paths for an example mouse during laser off and on in the open field (left), and distance traveled in the center as a function of light by virus type (right) (Arch n = 10; eYFP n = 10; two-way ANOVA interaction of light and virus $F_{(1,39)} = 5.84$ $p < 0.05$; **$p < 0.01$, *$p < 0.05$, t test).

(E) Latency to eat pellet in novelty suppression feeding test (Arch n = 8; eYFP n = 9; two-way ANOVA interaction of light and virus $F_{(1,33)} = 4.66$ $p < 0.05$, **$p < 0.005$, t test).

(F) Open arm avoidance in mediodorsal thalamus (MD) Arch- and eYFP-expressing animals (Arch n = 7; eYFP n = 4; p = 0.90). Data are presented as mean ± SEM throughout. See also Figures S1 and S2.

we compare unilateral versus bilateral vHPC-mPFC inhibition to distinguish physiological changes that are the direct consequence of the circuit manipulation from those that are secondary to changes in behavioral state. We find that vHPC inputs to the mPFC are required for anxiety-related behavior as well as spatial representations of aversion in mPFC neurons, while facilitating neural synchrony in a frequency- and pathway-specific manner.

RESULTS

vHPC Input to the mPFC Is Required for Anxiety-Like Behavior

To examine the role of the direct vHPC-to-mPFC pathway during anxiety-like behavior, vHPC terminals in the mPFC were inhibited using an optogenetic approach. An adeno-associated virus (AAV) carrying either the inhibitory opsin, enhanced Archeorhodopsin 3.0 (Arch), or enhanced yellow fluorescent protein (eYFP) under the control of the CamKIIα promoter was injected bilaterally into the vHPC of wild-type mice (Figure 1A). Optical fibers were implanted in the mPFC, along with microelectrodes in the mPFC, vHPC, and BLA. Seven weeks were allowed for viral expression to achieve maximal opsin levels in vHPC terminals within the mPFC (Figure 1B); we have previously shown that this approach results in at least a 40% reduction in effective neurotransmission in vivo (Spellman et al., 2015). Mice were then tested in the EPM for 8 min, with alternating 2-min periods of no illumination and illumination of the mPFC with green (532 nm) light (Figure 1C). In mice expressing Arch, but not those expressing eYFP alone, bilateral inhibition of vHPC terminals in the mPFC decreased open arm avoidance, as evidenced by both entries into and increased time spent in the open arms (Figure 1C). Bilateral inhibition of vHPC terminals in the mPFC also decreased center avoidance in the open field test (Figure 1D) and decreased latency to eat in the novelty suppression feeding test (Figure 1E), only in the Arch group. Locomotion and velocity were not affected by illumination in either eYFP or Arch mice (Figure S1).

To control for the non-specific effects of decreased excitation in the mPFC, Arch was used to inhibit inputs from the mediodorsal nucleus of the thalamus (MD) (Figure S2C). The strength of MD inputs onto mPFC neurons approximates that of vHPC inputs (Little and Carter, 2012). Bilateral inhibition of MD inputs to the mPFC had no effect on open arm avoidance (Figure 1F), suggesting that the behavioral effects of vHPC terminal inhibition are not solely due to a non-specific decrease in excitatory input.

vHPC Input to the mPFC Is Required for Theta-Frequency Long-Range Synchrony during Anxiety

The effects of bilateral vHPC-mPFC terminal inhibition on activity and synchrony within the extended vHPC-BLA-mPFC circuit were examined by recording single units in the mPFC and local field potentials (LFPs) in the mPFC, BLA, and vHPC. LFPs predominantly reflect summed synaptic activity within a brain region (Buzsáki et al., 2012). The temporal relationship between spikes

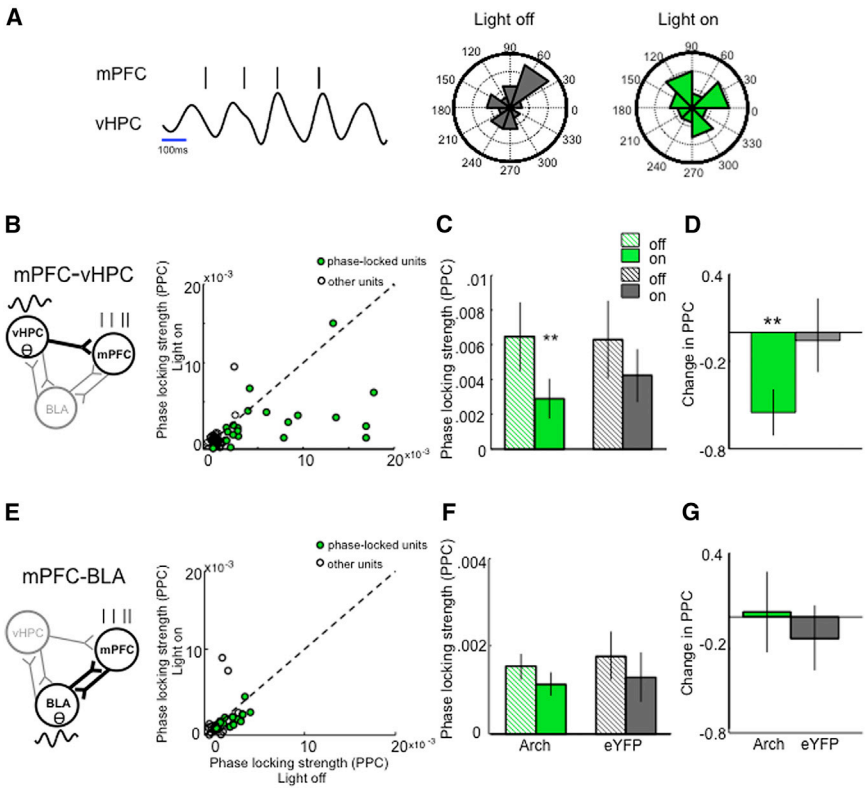

Figure 2. Inhibition of Hippocampal-Prefrontal Input Disrupts Synchrony of mPFC Units to vHPC but Not BLA Theta

(A) (Left) Representative raster plot of mPFC unit spiking in phase with simultaneously recorded vHPC theta oscillation. (Right) Distribution of vHPC theta phases on which this unit spiked during light off and light on epochs. Outer ring indicates 30% of spikes.

(B) Strength of phase locking (PPC) of mPFC units to vHPC theta with light on and light off; Arch animals only; n = 76. Green circles, significantly phase-locked units ($p < 0.05$, Rayleigh's test).

(C) Phase locking strength as a function of light for significantly phase-locked Arch and eYFP units (**p = 0.007, Wilcoxon sign rank test; total recorded Arch n = 76; eYFP n = 75).

(D) Normalized change in phase locking with illumination (significantly different from zero Arch p = 0.0015, eYFP p = 0.97, Wilcoxon sign rank).

(E–G) As in (B)–(D), for phase-locking of mPFC units to BLA theta (total recorded Arch n = 44; eYFP n = 22). See also Figures S3–S5.

and/or LFP activity in one region and LFPs in another can be used as a measure of synchrony (Harris and Gordon, 2015; Siapas et al., 2005). Terminal inhibition in the EPM decreased synchrony in the theta-frequency range between the vHPC and mPFC, as measured by the strength of phase locking of mPFC spikes to theta oscillations in the vHPC LFP (Figures 2B–2D). Phase locking of mPFC spikes to BLA theta was unaffected by terminal inhibition (Figures 2E–2G), demonstrating pathway specificity of the vHPC terminal inhibition. However, phase-locking to BLA was considerably weaker than to vHPC, allowing for a possible floor effect.

Synchrony was further examined using the LFPs recorded from each brain region. Consistent with decreased phase locking of mPFC spikes to vHPC theta, terminal inhibition decreased the correlation of theta power between the mPFC and vHPC (Figures S3A and S3D). This effect was specific to the closed arms of the EPM, consistent with previous reports showing that theta power correlation is higher in the safe compartments of the task (Adhikari et al., 2010; Likhtik et al., 2014). Terminal inhibition had no effect on theta power correlations in a familiar, non-aversive environment (Figure S4B), demonstrating task specificity.

The disruption in vHPC-mPFC theta power correlation was also frequency and pathway specific. Inhibiting vHPC terminals did not affect mPFC-vHPC power correlations in the delta (1–4 Hz), beta (13–30 Hz), or slow gamma (30–70 Hz) frequency ranges (Figure S4D). This frequency specificity is consistent with previous reports showing that anxiety does not modulate vHPC-mPFC synchrony in frequency ranges other than theta (Adhikari et al., 2010). mPFC-BLA theta power correlations were unaffected by vHPC-mPFC terminal inhibition (Figures S3C and S3F). Similarly, there was no overall effect on vHPC-BLA theta power correlations (Figure S3B), though a decrease in theta power correlation could be detected when analysis was restricted to data from the closed arms (Figure S3E). These findings reinforce the pathway specificity of the manipulation. Notably, coherence, a measure of phase synchrony, between LFPs in the vHPC and mPFC was not affected by the manipulation (Figure S4C), consistent with our previous findings that anxiety does not alter coherence (Adhikari et al., 2010). Together, these findings demonstrate that terminal inhibition functionally disconnects the mPFC from the vHPC during anxiety-like behavior, particularly disrupting communication in the theta-frequency range.

Interestingly, two measures of local synchrony within the mPFC were increased by terminal inhibition. Both correlated firing of simultaneously recorded mPFC single units (Figure S5A) and phase-locking of mPFC single units to mPFC fast gamma (70–120 Hz) (Figure S5B) were increased by illumination in Arch- but not eYFP-expressing animals. These findings raise the possibility that when decoupled from vHPC inputs, mPFC neuronal spiking synchronizes more strongly with local inputs.

Spatial Representations of Aversion in mPFC Neurons Require vHPC Input

To address if vHPC input is necessary for spatial representations of aversion, we turned to unilateral inhibition. Aversion in the EPM is determined by arm-type; the strength of mPFC representations of arm-type varies with avoidance behavior (Adhikari et al., 2011). Therefore, behavioral effects of the bilateral inhibition could confound physiological findings. To eliminate this confound, mPFC single-unit activity was recorded during unilateral inhibition of the vHPC-to-mPFC pathway in an additional

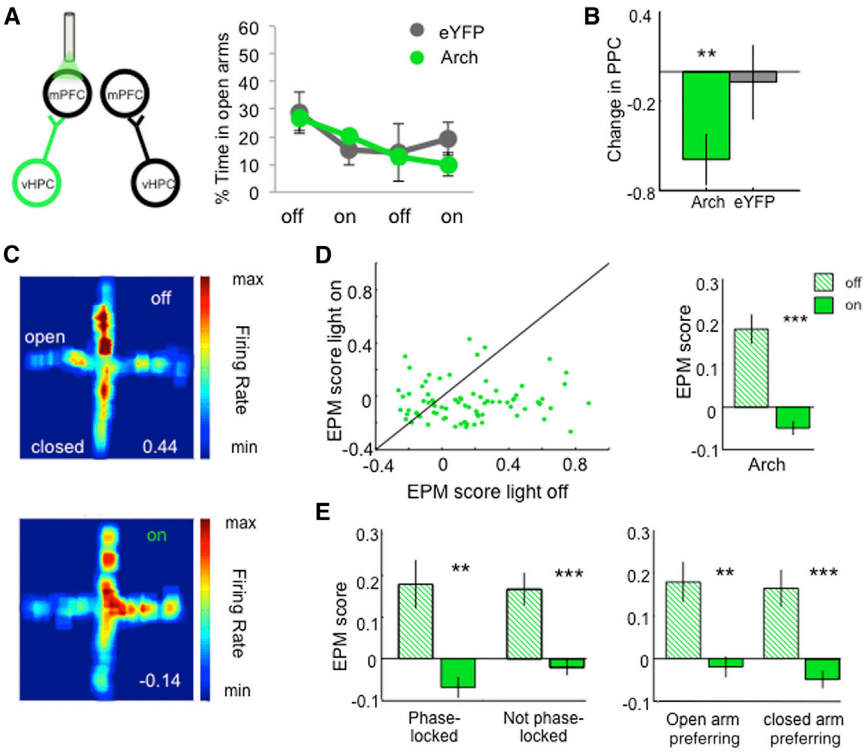

Figure 3. Unilateral Inhibition of Hippocampal-Prefrontal Input Disrupts Single-Unit Representations of Arm Type in the mPFC

(A) Avoidance behavior during unilateral inhibition of vHPC-mPFC input.

(B) Change in theta phase-locking strength in significantly phase-locked units during unilateral inhibition (Arch n = 16, $p < 0.01$; eYFP n = 11, $p = 0.4258$; Wilcoxon one-sample test).

(C) Firing rate map as a function of light for an example mPFC single unit. Top, light off; Bottom, light on. EPM score (see text) at bottom right.

(D) EPM score during light on versus light off epochs, for all mPFC single units from Arch mice. Right, mean EPM score as a function of light for units from Arch mice (n = 82, $p = 4.1 \times 10^{-7}$, Wilcoxon sign rank).

(E) Mean EPM score as a function of light for units characterized by significant phase-locking to vHPC theta (left) or by preferred arm type (right). $^{**}p < 0.01$; $^{***}p < 0.001$; Wilcoxon sign rank paired test.

cohort. As predicted, unilateral vHPC terminal inhibition did not affect avoidance behavior (Figure 3A). However, unilateral inhibition did disrupt phase locking of mPFC spikes to vHPC theta (Figure 3B) to a similar degree as did bilateral inhibition. Thus, unilateral inhibition successfully separates the physiological and behavioral effects of disrupting the vHPC-mPFC circuit.

Unilateral inhibition of vHPC-mPFC inputs abolished the representation of aversion in mPFC single units, as measured by the EPM score, which reflects arm-type selectivity (see Experimental Procedures; Figures 3C–3E). Mean EPM score was decreased regardless of whether the units were significantly phase-locked to vHPC theta or whether they fired preferentially in the open or closed arms (Figure 3F). Terminal illumination in mice expressing eYFP only did not affect EPM scores (Figure 4A). The decrease in arm-type representation was not simply due to a non-specific loss of excitation, since inhibiting the MD-mPFC pathway did not affect EPM scores (Figure 4B).

To further examine the contribution of vHPC input toward mPFC unit activity during EPM exploration, firing rates were examined. Each unit was classified as open- or closed-arm preferring, depending on where the firing rate was highest for that unit. Overall firing rates did not change with terminal inhibition for all neurons (Figure 5A) or for putative interneurons or pyramidal neurons (data not shown). However, firing rates in the preferred arm type decreased with vHPC inhibition for both open- and closed-preferring units (Figures 5B–5G), suggesting that the net effect of vHPC input is excitatory.

These findings suggest that direct vHPC inputs provide patterned excitation that is required for mPFC spatial representations of aversiveness in the EPM. However, mPFC neurons can represent task-relevant information in a variety of tasks. To determine whether vHPC input is important for mPFC representations of a similar, but non-aversive context, a modified neutral plus maze was created. In this maze, all four arms were fully enclosed, and the two types of arms were marked by different visual patterns (see Experimental Procedures). An additional cohort of mice were implanted and recorded during exploration of this neutral maze. Mice did not display a preference for either arm type (58% ± 12% and 42% ± 12% time spent in each arm type, respectively; $p = 0.40$). mPFC units only weakly represented arm-type in this neutral maze compared to the the EPM (Figures 6A and 6B). Moreover, the EPM scores in the neutral maze were not statistically different from EPM scores generated from shuffled spikes (Figure 6C), suggesting that mPFC representations of arm-type in this neutral maze are minimal. Even so, inhibition of the vHPC-to-mPFC pathway decreased the mean EPM scores significantly (Figures 6D–6F).

Bilateral Terminal Inhibition Reduces Behavioral and Physiological Markers of Anxiety

The effects of terminal inhibition on arm-type representations in the neutral maze were small. Nonetheless, they raise the question of whether inhibition of vHPC input to the mPFC alters the anxiety state of the animal or simply disrupts spatial information without affecting valence. To address this issue, we compared additional behavioral and physiological markers of anxiety state across the unilateral and the bilateral terminal inhibition experiments.

Behaviorally, we examined head dips in the open arms and the duration of open arm visits. The number of head dips over the open arm edge is associated with anxiety behavior in the EPM (Rodgers and Johnson, 1995). We reasoned that if spatial representations alone were disrupted, without altering anxiety per se, the mice would continue to avoid head dips and make rapid exits from the open arms, despite bilateral inhibition of

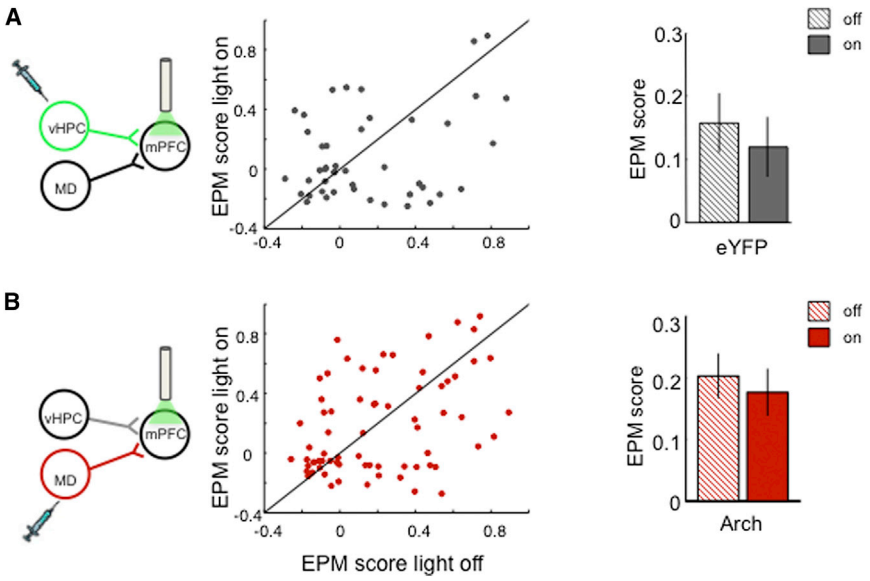

Figure 4. Disruption of Arm-Type Representations Requires Active Inhibition and Is Input Specific

(A and B) Effect of unilateral mPFC illumination on EPM scores in mice expressing eYFP in vHPC (A) (n = 48, p = 0.44, Wilcoxon sign rank paired test) or Arch in MD (B) (n = 74, p = 0.68; Wilcoxon sign rank paired test).

the vHPC-mPFC pathway. However, bilateral inhibition of the vHPC-mPFC pathway increased both the total number of head dips and the frequency of head dips per unit time spent in the open arms; unilateral inhibition had no effect on these measures, as expected (Figure 7A). Similarly, bilateral, but not unilateral, inhibition increased the duration of open arm visits (Figure 7B). Terminal illumination in eYFP-expressing mice had no effect on either behavior. These findings suggest that with bilateral (but not unilateral) terminal inhibition, mice fail to treat the open arms as aversive.

Physiologically, we took advantage of previously established markers of anxiety in the amygdala and mPFC LFPs. Fear conditioning and open field exposure induce characteristic patterns of neural activity in the BLA and mPFC (Lesting et al., 2011; Likhtik et al., 2014; Stujenske et al., 2014). Specifically, in addition to the increased theta activity and synchrony discussed above, the strength (power) of fast gamma-frequency (70–120 Hz) oscillations in the BLA and mPFC decrease during anxiety and increase during relative safety (Stujenske et al., 2014). Within the BLA, the strength of the relationship between theta- and gamma-frequency oscillations is increased with anxiety and decreased with relative safety (Stujenske et al., 2014). Accordingly, exposure to the EPM decreased fast gamma power and increased theta-gamma coupling compared to a baseline safe condition (Figure S6). If inhibition of the vHPC-mPFC pathway is truly anxiolytic, we would expect that bilateral inhibition would reduce these physiological markers of anxiety.

Indeed, bilateral terminal inhibition mimicked the effects of relative safety on each of these parameters. Bilateral inhibition increased the strength of gamma oscillations in the BLA and mPFC (Figure 7C), inducing a shift in the directionality of gamma synchrony toward increased mPFC lead (Figure 7D). Bilateral inhibition also reduced the strength of coupling between theta and gamma oscillations within the BLA (Figure 7E). Unilateral inhibition, however, did not alter any of these parameters in the inhibited hemisphere (Figures 7F–7H), nor did illumination in YFP-expressing mice (Figure S7).

The unilateral inhibition experiments are particularly important for evaluating the physiological markers, as they allow one to distinguish between direct effects of the manipulation on the circuit and indirect effects of the behavioral changes induced by the manipulation. If BLA and mPFC gamma alterations were directly caused by inhibiting vHPC input to the mPFC, then unilateral inhibition would have altered these parameters in the absence of changes in behavior. The lack of effect of unilateral inhibition demonstrates that BLA and mPFC gamma strength, mPFC-to-BLA gamma directionality, and BLA theta-gamma coupling reflect the behavioral state of the animal and not simply decreased vHPC-mPFC input.

These behavioral and physiological findings support the notion that bilateral inhibition of vHPC-mPFC terminals alters the anxiety state of the animal, rather than simply altering arm-type selection.

DISCUSSION

The findings described here demonstrate that the direct vHPC-to-mPFC pathway is necessary for anxiety-related behavior, vHPC-mPFC theta synchrony, and spatial representations of aversion in the mPFC. Intriguingly, this inhibition resulted in frequency-specific and pathway-specific effects. Moreover, though vHPC input is required for both anxiety-related and valence-free representations in the mPFC, both behavioral and physiological evidence suggest decreases in anxiety with terminal inhibition. Together, these findings suggest a model in which behaviorally relevant contextual information from the vHPC is sent to the mPFC and utilized to guide avoidance behavior; theta-frequency synchrony appears to be important for this process. The implications of these findings, particularly in terms of the extended BLA-vHPC-mPFC circuit, are discussed below.

Synchrony in the vHPC-mPFC-BLA Circuit

The BLA, vHPC, and mPFC comprise a tripartite circuit in which each element is important for anxiety-like behavior. Silencing or lesioning any of these three structures alters avoidance behavior in tests such as the EPM (Jinks and McGregor 1997;Kjelstrup et al., 2002; Shah and Treit, 2003; Bannerman et al., 2003). Similarly, optogenetically manipulating BLA inputs into the vHPC (Felix-Ortiz et al., 2013) or the mPFC (Felix-Ortiz et al., 2015) alters anxiety. However,

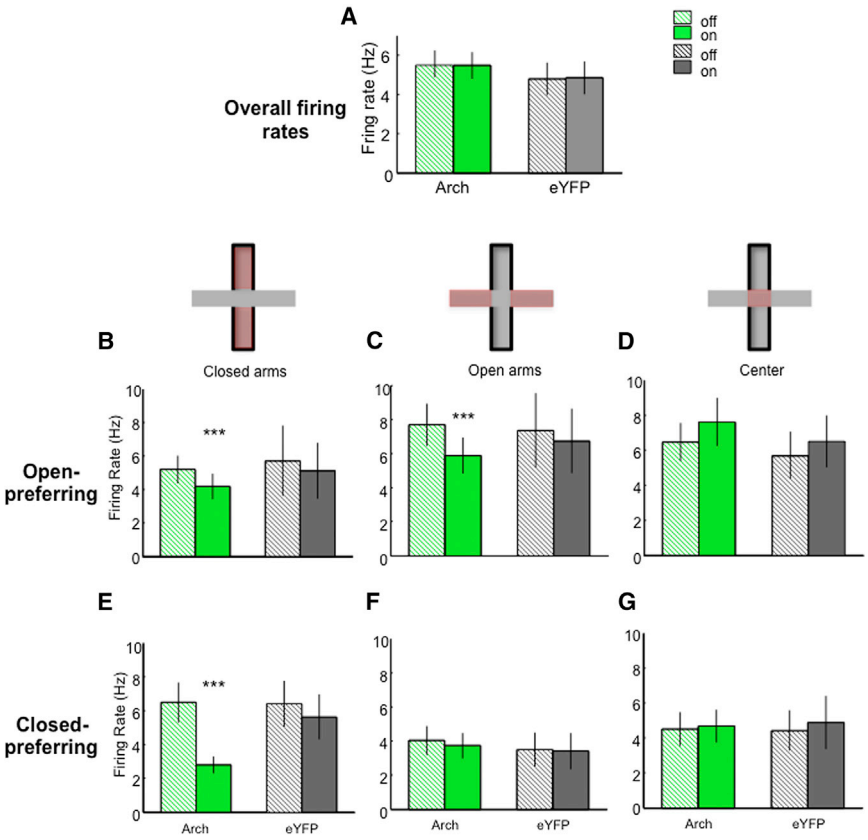

Figure 5. Inhibition of Hippocampal-Prefrontal Input Decreases mPFC Neuronal Firing Rates in the Preferred Arms

(A) Overall firing rate in the EPM (Arch n = 82 and eYFP n = 46).

(B–D) Firing Rate for open-preferring units in the closed arms (B) (Arch n = 42, $p < 0.001$; eYFP n = 26, $p = 0.46$; Wilcoxon sign rank paired test), open arms (C) (Arch n = 42, $p < 0.001$; eYFP n = 20, $p = 0.55$; Wilcoxon sign rank paired test), and center (D).

(E–G) Firing rate for closed-preferring units in the closed arms (E) (Arch n = 40, $p < 0.001$; eYFP n = 20, $p = 0.12$), open arms (F), and center (G).

these structures are intimately interconnected (Hoover and Vertes, 2007; Pikkarainen et al., 1999), as evidenced by the remarkable degree of synchrony that arises during fear and anxiety behaviors (Adhikari et al., 2010; Lesting et al., 2011; Likhtik et al., 2014; Seidenbecher et al., 2003; Stujenske et al., 2014). Thus, manipulations of any one structure could alter activity patterns in any other within the circuit; the specificity of such manipulations is questionable. Here we attempt to address this caveat by recording simultaneously from the three structures. Inhibition of the vHPC terminals within the mPFC was relatively specific, disrupting synchrony in the theta frequency range between the vHPC and the mPFC with minimal effects on theta synchrony between the BLA and either structure. Importantly, phase-locking of mPFC units to vHPC theta was reduced in both unilateral and bilateral silencing experiments, demonstrating that reduced theta synchrony is a primary effect of inhibiting vHPC input. By contrast, only bilateral inhibition had effects on BLA and mPFC gamma strength and synchrony, suggesting that these measures may be readouts of the anxiety state rather than being causally involved in generating it.

The effects of terminal inhibition on vHPC-mPFC interactions were remarkably specific. Theta- synchrony was unaffected in a familiar, non-aversive environment, arguing that vHPC input is required for the increase in synchrony seen in the EPM; indeed, terminal inhibition completely wipes out the fold increase in power correlation from the familiar environment to the EPM (compare Figure S4B to Figure S3). The effects on LFP synchrony were confined to the closed arms, consistent with our prior findings (Adhikari et al., 2010), suggesting that vHPC-mPFC interactions are particularly engaged during periods of active inhibition of exploration. We also found deficits in LFP synchrony were limited to effects on power correlations, without any effects on coherence. While consistent with prior findings that coherence is unaffected by anxiety (Adhikari et al., 2010), the different effects on these two measures caution against simplistic interpretations based on measures of synchrony that rely solely on LFPs. The phase-locking data presented here are therefore particularly important in demonstrating effective disruption of connectivity.

The Origin of Spatial Representations of Aversion in the mPFC

Inhibition of the direct vHPC input ablated the representation of aversive and non-aversive context within the mPFC. This result is consistent with recent findings during a working memory task, in which the representation of goal location was disrupted by the same manipulation (Spellman et al., 2015). However, mPFC units encode valence; neurons that fire in response to bright, enclosed arms also fire in response to open arms in the dark (Adhikari et al., 2011). Moreover, terminal inhibition altered additional behavioral measures of valence, independent of arm choice, suggesting that vHPC inputs are crucial not just for spatial representations but also for the anxiety valence. Whether this valence is constructed in the mPFC with the help of vHPC input or is present in the vHPC itself is unclear. A recent report demonstrates that mPFC-projecting vHPC neurons preferentially encode arm type in the EPM, while very few have well-defined place fields (Ciocchi et al., 2015). Evidence from human hippocampal imaging suggests that the anterior hippocampus (the human homolog of the vHPC) responds to negative valence (Gerdes et al., 2010; Sterpenich et al., 2014). These findings suggest the possibility that vHPC inputs indeed convey valence information to the mPFC. Where might the vHPC get information about

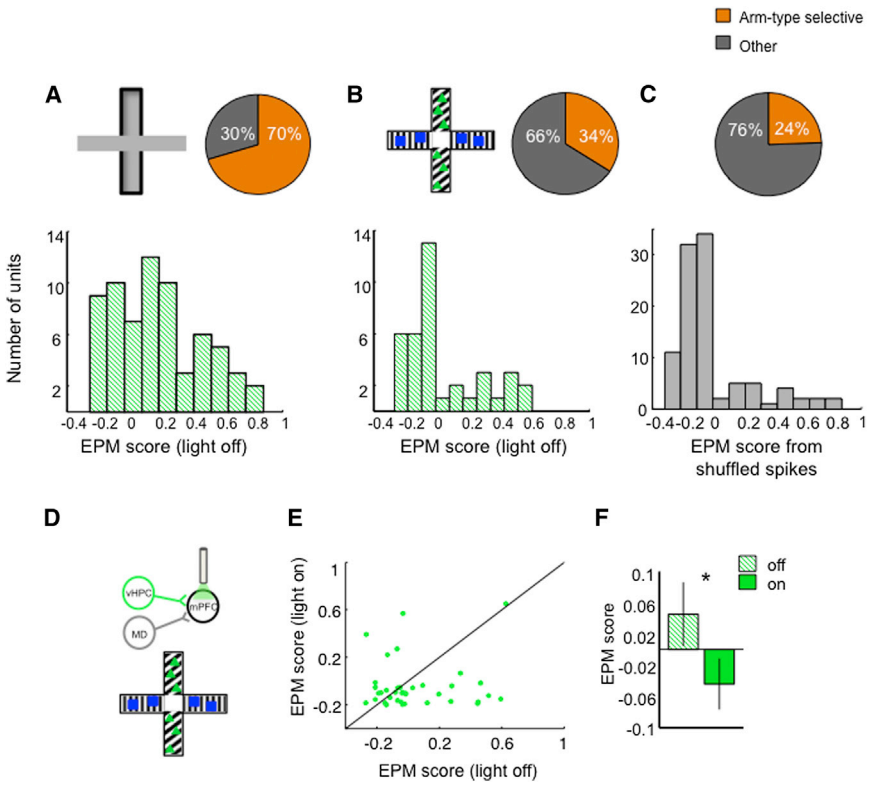

Figure 6. Arm-Type Representations in a Non-Aversive Environment

(A–C) Distribution of arm-type selective cells in the standard EPM (A), a modified, non-aversive maze (B), and 100 EPM scores generated from randomly shuffled spikes from the standard EPM data (C). Top, schematics of mazes, and percentage of cells with EPM scores > 0 ("arm-type selective," orange). Bottom, full distribution of EPM scores for each condition. The distributions in (A) and (B) are significantly different from each other (standard EPM, n = 64; non-aversive, n = 40; Kolmogorov-Smirnov test p = 0.002). The distribution in (B) and (C) are not significantly different from each other (Kolmogorov-Smirnov test p = 0.63).

(D) Schematic of unilateral vHPC-mPFC inhibition in the modified maze.

(E) Scatter plot of EPM scores for individual single units with and without illumination in the neutral maze.

(F) Mean EPM score of mPFC units with and without unilateral inhibition of vHPC-mPFC (Arch n = 40 units, sign rank *p < 0.05).

valence? It could come from the BLA, given the demonstration that optogenetic inhibition of BLA terminals within the vHPC also disrupts anxiety-like avoidance behavior (Felix-Ortiz et al., 2013).

Is the Role of vHPC-mPFC Input the Same in Learned and Innate Forms of Anxiety?

In addition to innate forms of anxiety, such as those tested in the EPM, learned fear also engages the vHPC-mPFC circuit. In learned fear paradigms, silencing the vHPC, similar to the BLA, disrupts both the expression (during fear recall) and suppression (during extinction recall) of fear (Maren and Holt, 2004; Sierra-Mercado et al., 2011). These reports suggest that the role of the vHPC during learned fear may be more complex than during innate anxiety. Similarly, the influence of vHPC input on mPFC unit activity may differ with the behavioral paradigm used. Silencing the vHPC during learned fear recall results in increased mPFC single-unit responses to the conditioned stimulus (Sotres-Bayon et al., 2012), suggesting an inhibitory role for the vHPC projection. Here, inhibiting vHPC input resulted in decreased neuronal activity within a neuron's preferred arm, suggesting an excitatory role (Figure 5). These opposite results may be due to differences in experimental methods—Sotres-Bayon et al. (2012) used muscimol in the vHPC, which silences all projections, while here only those projections to the mPFC are inhibited. Alternatively, they may be genuine, task-related differences between learned and innate forms of anxiety.

At least for innate anxiety, as demonstrated here, it does appear that the predominant effects of vHPC input are excitatory and, in particular, that this excitation boosts firing rates specifically in each neuron's preferred arm. This data are consistent with findings during a spatial working memory task, which indicate that inhibiting vHPC terminals eliminates the boost in firing that occurs in mPFC neurons in their preferred goal locations (Spellman et al., 2015).

CONCLUSION

A long literature links theta-frequency synchrony between the vHPC, mPFC, and BLA to both learned fear and innate anxiety (Adhikari et al., 2011; Lesting et al., 2011; Likhtik et al., 2014; Seidenbecher et al., 2003; Stujenske et al., 2014). Indeed, directly manipulating theta-frequency oscillations within the mPFC induces freezing, suggesting a causal relationship between theta and fear (Courtin et al., 2014). Here, inhibition of the vHPC-to-mPFC pathway decreased avoidance behavior and disrupted theta-frequency synchrony between the two structures without affecting synchrony at other frequencies. This specificity is consistent with the frequency-specific increases in synchrony seen during anxiety (Lesting et al., 2011; Likhtik et al., 2014; Seidenbecher et al., 2003; Stujenske et al., 2014). Interestingly, inhibition of this same vHPC-to-mPFC pathway during a working memory task had no effect on theta-frequency synchrony (Spellman et al., 2015); instead, low gamma (30–70 Hz) synchrony was specifically disrupted. These contrasting findings demonstrate the surprising result that a specific anatomical pathway can mediate synchrony at different frequencies depending on behavioral state. They further suggest the exciting proposition that disrupting theta-frequency communication in this pathway could have anxiolytic effects without impairing hippocampal-prefrontal-dependent cognition.

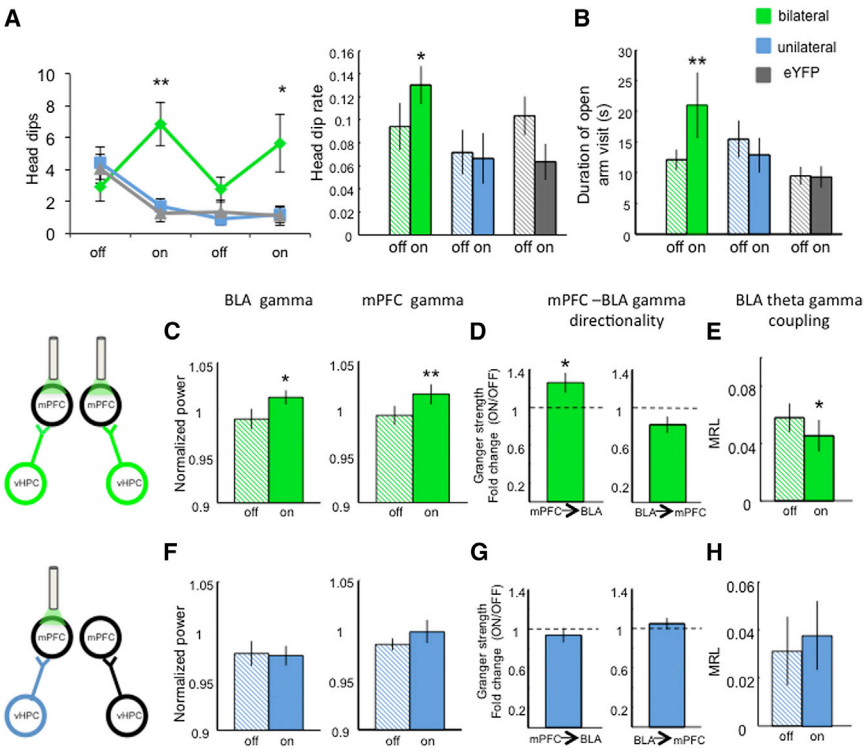

Figure 7. Behavioral and Physiological Evidence of Decreased Anxiety during Bilateral, but Not Unilateral, vHPC-mPFC Inhibition

(A) Left, head dips during bilateral (green) versus unilateral (blue) inhibition (n = 12 per group; two-way rmANOVA, interaction of light and group, $F_{(2,24)} = 8.74$, $p < 0.001$; bilateral versus unilateral inhibition, $p < 0.01$, post hoc Wilcoxon rank-sum). Right, frequency of head dips (total head dips/time in open arms) as a function of illumination (effect of light in bilateral group, $p = 0.03$, Wilcoxon paired test).

(B) Duration of open arm visits as a function of illumination (effect of light in bilateral group, $p = 0.0063$, Wilcoxon paired test).

(C–H) Effect of bilateral (green, [C]–[E]) versus unilateral (blue, [F]–[H]) terminal inhibition on fast gamma power in the BLA and mPFC ([C] and [F]) (*n = 8, $p = 0.04$; **n = 10, $p = 0.009$; Wilcoxon paired test), Granger causality (*n = 8, $p = 0.039$, Wilcoxon one sample test) ([D] and [G]) and BLA theta/gamma coupling ([E] and [H]). (*n = 8, $p = 0.01$, Wilcoxon paired test). See also Figures S6 and S7.

EXPERIMENTAL PROCEDURES

Subjects

A total of 68 adult male 129SvevTac mice (Taconic Farms) were used for the vHPC experiments, and an additional 15 adult male C57Bl/6 mice (Jackson Labs; RRID: IMSR_JAX:000664) were used for the MD thalamus experiments. All mice were aged 8–12 weeks at the start of the experiments. All procedures described were done in accordance with guidelines from and approved by the IACUCs of both Columbia University and the New York State Psychiatric Institute.

Surgical Procedures

For the vHPC experiments, mice were unilaterally or bilaterally infected (n = 29 and 23, unilateral and bilateral, respectively) with either AAV5 CamKIIα-eArch3.0-eYFP or AAV5 CamKIIα–eYFP into the vHPC under isoflurane anesthesia. 200 nl of 10^{12} vg/ml virus was pressure-injected through a glass micropipette. In each hemisphere, six injections were done at −3.10 and at −3.30 AP levels for a total of 12 injections per hemisphere. At each AP level, the six injection sites were 2.90, −4.0; ±2.90, −1.55; ±3.30, −3.60; ±3.30 −1.7; ±3.70, −3.2; ±3.70, −2.5 (ML and DV, respectively). Coordinates are in mm relative to Bregma (AP, ML) or brain surface (DV). All viruses were obtained from the University of North Carolina Vector core. Virus was infused at a rate of 100 nl/min. Using this protocol we have recently demonstrated that vHPC terminal inhibition in the mPFC decreases vHPC stimulation-evoked firing rates by approximately 40% in vivo (Spellman et al., 2015).

6–8 weeks after viral infection, electrodes and optical fibers were implanted in a second surgery, also under isoflurane anesthesia. Stereo-optrodes were implanted in the mPFC (AP −1.65 ML ±0.4 DV −1.25). Each stereo-optrode was comprised of a 230 um optical fiber glued to a bundle of 14 tungsten wire (13 μM diameter) stereotrodes placed 400–500 μm below the end of the optical fiber. 75 μM diameter tungsten wire LFP electrodes were implanted in the BLA (AP −1.80, ML ±3.16, DV −4.10) and the CA1 region of the vHPC (AP −3.30, ML ±3.30, DV −3.60). A reference screw was implanted in the skull over the frontal cortex and a ground screw in the skull over the cerebellum.

For the MD experiments, AAV5-hSyn-eArch3.0-eYFP or AAV5-hSyn-eYFP was used. 200 nl volume of [10^{12} vg/ml] virus was injected into the MD of 15 mice (AP −1.2, ML ± 0.35, DV −3.2). Eleven mice were used to determine the effects of bilateral MD-mPFC inhibition on avoidance behavior (Figure 1E). Four mice were used to determine the effects of unilateral inhibition on arm type representations in mPFC neurons (Figure 4G). The mice utilized in the unilateral experiment underwent training and testing in a spatial working memory task 4 weeks prior to the exposure to the EPM.

Behavior

5–7 days after electrode microdrive implantation, mice were food restricted to 80% of pre-operative weight and habituated to the opto/electrical tether in a small dark wooden box (20 × 30 cm) as they foraged for food pellets. On the fifth day of habituation, after 1 hr rest, mice were placed in the EPM under 300 lux illumination. Five mice were excluded from behavioral analysis for having less than 3 s of exploration in the open arms throughout the duration of the experiment. Behavior in the EPM was hand scored to ensure consistency of analysis. A mouse was said to be inside an open or closed arm if all four paws were inside the arm. Head dips were defined as the full head of mouse coming out of open arm borders; this head-dipping behavior is quantified and described in Rodgers and Johnson (1995). For the non-aversive maze experiment (Figure 6), an EPM under ~100 lux illumination was modified such that all arms were closed. The walls of two arms were covered with vertical stripes and blue squares while the walls of the other two arms were covered with diagonal stripes and green triangles (58% ± 12% and 42% ± 12% time spent in each arm type, respectively; $p = 0.40$). To test significance of behavioral changes, two-way repeated-measures ANOVAs with post hoc, Bonferroni corrected t tests were used. The laser output was controlled using Neuralynx Trial Control (Neuralynx) to deliver constant 532 nm light at 10 mW (measured at the tip of the optical fiber) every 2 min. To test additional anxiety assays a cohort of 16 mice was injected with AAV5 CamKIIα-eArch3.0-eYFP or AAV5 CamKIIα-eYFP and implanted with bilateral optical fibers in mPFC (see Surgical Procedures for coordinates). After 7 to 8 weeks of viral expression, the mice were tested in the open field (25 cm radius, 40 cm high) under 80 lux illumination for 8 min with the same laser

protocol as the EPM. For the novelty-suppressed feeding test, animals were food restricted for 24 hr and placed in a 40 × 60 cm brightly lit arena (200–250 lux) with a food pellet placed on filter paper in the center of the arena. The trial was terminated either when an animal began chewing or when 600 s transpired, whichever occurred first. Immediately after terminating the trial, animals were then placed in their home cage and the amount of food consumed in 5 min was measured (home cage consumption), followed by an assessment of post-restriction weight. The task was repeated twice on different days for each mouse, counterbalanced for light stimulation (ON) or no stimulation (OFF). Percentage body weight lost during food deprivation prior to the testing was assessed to ensure both groups lost similar amounts of weight, and home cage consumption immediately after testing was assessed as a relative measure of hunger (mg pellet consume/mouse weight). Neither variable was affected by illumination in either eYFP or Arch animals.

Data Acquisition

Electrophysiological data were acquired using a Digital Lynx system (Neuralynx). LFPs were referenced to a screw located in the skull over the frontal cortex/olfactory bulb, band-pass filtered (1–1,000 Hz), and acquired at 2 kHz. Unit recordings were band-pass filtered at 600–6,000 Hz and acquired at 32 kHz; spikes were detected by thresholding and sorted off-line. Initial automated spike sorting was done based on peak, energy and principal component analysis, using Klustakwik (Ken Harris, UCL) instantiated in SpikeSort3D (Neuralynx); clusters were subsequently manually confirmed. Isolation distance and L-ratio were computed as described in Schmitzer-Torbert et al. (2005). The median Isolation distance for the single-unit clusters was 26, and the median L-ratio was 0.08.

LFP Analysis

All data were analyzed using custom-written scripts in MATLAB (MathWorks). Power correlations were computed as previously described (Adhikari et al., 2010). Briefly, we determined power as a function of time using the multitaper method, with window sizes customized for each frequency range. Window sizes for the power correlation were 2.5, 1, and 0.125 s for theta (4–12 Hz), beta (13–20 Hz), and gamma (30–70 Hz) frequencies, respectively. Pearson's correlation was then used to measure the association between power across regions. To determine the strength of power correlations that would be expected by chance, we randomly shuffled the time windows in one brain region 2,000 times, calculating a Pearson's correlation each time. From these random distributions, we identified the 95% critical value for each frequency range; these were remarkably consistent at r = 0.142 to 0.150 for each frequency, averaging at 0.146 for theta, beta, slow, and fast gamma, and 0.147 for delta ranges. For open versus closed arm power correlation analysis, only mice that spent at least 3 s in each arm type during each light condition were included.

Coherence of mPFC and vHPC LFPs was estimated using the Welch method (mscohere function in MATLAB) with the same parameters used as for the power spectra. Fast gamma power was calculated for times the animal was in the closed arms of the EPM. LFPs from times spent in the closed arms of the EPM were filtered for 70–120 Hz, and power was calculated using a Hilbert transformation and normalized to fast gamma power throughout the session. To quantify theta-gamma coupling, we computed the mean resultant length (MRL) of fast gamma power as a function of theta phase for times spent in the closed arms of the EPM. Theta phase and gamma power were both calculated using the Hilbert transform. The MRL was chosen because of the observed unimodal relationship of theta phase-gamma amplitude coupling in gamma ranges and its higher statistical power compared to the non-parametric modulation index (Tort et al., 2009). Granger causality analysis was performed as described in Stujenske et al. (2014) using arfit toolbox for Matlab. The strength of mPFC granger lead was calculated as $GC_{mPFC\rightarrow(BLA/GC_{mPFC\rightarrow BLA}+GC_{BLA\rightarrow mPFC})}$ for each animal, and the strength of BLA granger lead was calculated as $GC_{BLA\rightarrow(mPFC/GC_{mPFC\rightarrow BLA}+GC_{BLA\rightarrow mPFC})}$.

Single-Unit Analysis

Only units with at least 100 spikes for each light condition were included. A given unit was said to be significantly phase locked if the distribution of the LFP phases where the spikes occurred was not uniform as assessed with Rayleigh's test for non-uniformity of circular data. Zero phase corresponds to the peak of the signal. Phase locking strength was quantified using pairwise phase consistency (PPC) (Vinck et al., 2010). To calculate the power envelope and phase of ongoing theta and gamma oscillations, a band-pass filter for 4–12 Hz was used using a zero-phase-delay FIR filter with Hamming window (filter0, provided by K. Harris and G. Buzsaki, New York University, USA), the phase component was calculated by a Hilbert transform, and a corresponding phase was assigned to each spike. Firing rate analysis was also conducted for putative interneurons versus pyramidal neurons, separated as previously described (Spellman et al., 2015).

The EPM score was calculated for each single-unit as previously described in Adhikari et al. (2011) (EPM Score = (A − B)/(A + B); where A = 0.25•(|FL − FU| + |FL − FD| + |FR − FU| + |FR − FD|) and B = 0.5•(|FL − FR| + |FU − FD|). FL, FR, FU, and FD are the percentage difference from mean firing rate in left, right, up and down arms, respectively). Only mice that explored each of the four arms on both light conditions for at least 4 s were included in the EPM score analyses. Firing rates for different compartments of the EPM was calculated as total spikes in that compartment divided by the time mouse spent in the compartment. To test the significance of phase-locking strength, EPM score, and firing rate analyses, the non-parametric Wilcoxon sign rank or rank-sum tests were used.

Statistics

To determine light effects on power correlations, cross-correlations, firing rate, MRL, EPM score, PPC, and gamma power, Wilcoxon (sign rank) paired tests were performed. The sign rank test does not assume normality in the data and is meant for paired samples. To determine fold changes or percentage changes in PPC and Granger lead strength, Wilcoxon one-sample tests were performed. To determine if the distributions of EPM scores (Figure 6) were different from each other, Kolmogorov-Smirnov tests were performed. Finally, to determine light effects on the behavioral results, repeated-measures two-way ANOVAs were performed along with post hoc Bonferroni corrected t tests. Sample sizes and p values are reported in the figure legends.

Histology

Recording sites were histologically confirmed by visual examination of electrolytic lesions. Lesions were induced immediately before perfusions by passing current through an electrode at each implanted site (50 μA, 20 s). Perfused and fixed tissue was then sectioned and mounted with DAPI Fluoromount-G mounting medium (Southern Biotech). Native fluorescence of Arch and eYFP was imaged using an epifluorescence microscope.

SUPPLEMENTAL INFORMATION

Supplemental Information includes seven figures and can be found with this article online at http://dx.doi.org/10.1016/j.neuron.2016.01.011.

AUTHOR CONTRIBUTIONS

Conceptualization, N.P.-C. and J.A.G. Methodology, N.P.-C., S.S.B., G.M.P., A.L.G.-G., T.J.S., and J.A.G. Investigation, N.P.-C., S.S.B., G.M.P., D.R.B., W.D.H., and A.L.G.-G. Writing – Original Draft, N.P.-C. Writing – Review and Editing, N.P.-C., S.S.B., and J.A.G.

ACKNOWLEDGMENTS

We thank Avishek Adhikari, Rene Hen, Sarah Woolley, and members of the Gordon Lab for comments on the manuscript. We thank Mihir Topiwala for assistance with behavior. We thank Alexander Harris for advice regarding data analysis. We thank one of the anonymous reviewers for suggesting examining gamma power and synchrony in the BLA as markers of changes in anxiety state. N.P.-C. was supported by the National Science Foundation. A.L.G.-G. was supported by a Spanish Ministry of Science postdoctoral fellowship and a Sackler Institute Award. S.S.B. was supported by an NRSA from the NIMH (NIH F31MH102041). J.A.G. was supported by the

NIMH (MH081968 and MH096274), the Jerome Jacobson Foundation, the International Mental Health Research Organization, and the Hope for Depression Research Foundation.

Received: April 20, 2015
Revised: July 31, 2015
Accepted: December 24, 2015
Published: February 4, 2016

REFERENCES

Adhikari, A., Topiwala, M.A., and Gordon, J.A. (2010). Synchronized activity between the ventral hippocampus and the medial prefrontal cortex during anxiety. Neuron *65*, 257–269.

Adhikari, A., Topiwala, M.A., and Gordon, J.A. (2011). Single units in the medial prefrontal cortex with anxiety-related firing patterns are preferentially influenced by ventral hippocampal activity. Neuron *71*, 898–910.

Bannerman, D.M., Grubb, M., Deacon, R.M.J., Yee, B.K., Feldon, J., and Rawlins, J.N.P. (2003). Ventral hippocampal lesions affect anxiety but not spatial learning. Behav. Brain Res. *139*, 197–213.

Buzsáki, G., Anastassiou, C.A., and Koch, C. (2012). The origin of extracellular fields and currents–EEG, ECoG, LFP and spikes. Nat. Rev. Neurosci. *13*, 407–420.

Ciocchi, S., Passecker, J., Malagon-Vina, H., Mikus, N., and Klausberger, T. (2015). Brain computation. Selective information routing by ventral hippocampal CA1 projection neurons. Science *348*, 560–563.

Courtin, J., Chaudun, F., Rozeske, R.R., Karalis, N., Gonzalez-Campo, C., Wurtz, H., Adbi, A., Baufreton, J., Bienvenu, T.C.M., and Herry, C. (2014). Prefrontal parvalbumin interneurons shape neuronal activity to drive fear expression. Nature *505*, 92–96.

Felix-Ortiz, A.C., Beyeler, A., Seo, C., Leppla, C.A., Wildes, C.P., and Tye, K.M. (2013). BLA to vHPC inputs modulate anxiety-related behaviors. Neuron *79*, 658–664.

Felix-Ortiz, A.C., Burgos-Robles, A., Bhagat, N.D., Leppla, C.A., and Tye, K.M. (2015). Bidirectional modulation of anxiety-related and social behaviors by amygdala projections to the medial prefrontal cortex. Neuroscience. http://dx.doi.org/10.1016/j.neuroscience.2015.07.041.

Gerdes, A.B.M., Wieser, M.J., Mühlberger, A., Weyers, P., Alpers, G.W., Plichta, M.M., Breuer, F., and Pauli, P. (2010). Brain Activations to Emotional Pictures are Differentially Associated with Valence and Arousal Ratings. Front. Hum. Neurosci. *4*, 175.

Harris, A.Z., and Gordon, J.A. (2015). Long-range neural synchrony in behavior. Annu. Rev. Neurosci. *38*, 171–194.

Hoover, W.B., and Vertes, R.P. (2007). Anatomical analysis of afferent projections to the medial prefrontal cortex in the rat. Brain Struct. Funct. *212*, 149–179.

Jinks, A.L., and McGregor, I.S. (1997). Modulation of anxiety-related behaviours following lesions of the prelimbic or infralimbic cortex in the rat. Brain Res. *772*, 181–190.

Kjelstrup, K.G., Tuvnes, F.A., Steffenach, H.-A., Murison, R., Moser, E.I., and Moser, M.-B. (2002). Reduced fear expression after lesions of the ventral hippocampus. Proc. Natl. Acad. Sci. USA *99*, 10825–10830.

Lesting, J., Narayanan, R.T., Kluge, C., Sangha, S., Seidenbecher, T., and Pape, H.-C. (2011). Patterns of coupled theta activity in amygdala-hippocampal-prefrontal cortical circuits during fear extinction. PLoS ONE *6*, e21714.

Lesting, J., Daldrup, T., Narayanan, V., Himpe, C., Seidenbecher, T., and Pape, H.-C. (2013). Directional theta coherence in prefrontal cortical to amygdalo-hippocampal pathways signals fear extinction. PLoS ONE *8*, e77707.

Likhtik, E., Stujenske, J.M., Topiwala, M.A., Harris, A.Z., and Gordon, J.A. (2014). Prefrontal entrainment of amygdala activity signals safety in learned fear and innate anxiety. Nat. Neurosci. *17*, 106–113.

Little, J.P., and Carter, A.G. (2012). Subcellular synaptic connectivity of layer 2 pyramidal neurons in the medial prefrontal cortex. J. Neurosci. *32*, 12808–12819.

Maren, S., and Holt, W.G. (2004). Hippocampus and Pavlovian fear conditioning in rats: muscimol infusions into the ventral, but not dorsal, hippocampus impair the acquisition of conditional freezing to an auditory conditional stimulus. Behav. Neurosci. *118*, 97–110.

Pikkarainen, M., Rönkkö, S., Savander, V., Insausti, R., and Pitkänen, A. (1999). Projections from the lateral, basal, and accessory basal nuclei of the amygdala to the hippocampal formation in rat. J. Comp. Neurol. *403*, 229–260.

Rodgers, R.J., and Johnson, N.J. (1995). Factor analysis of spatiotemporal and ethological measures in the murine elevated plus-maze test of anxiety. Pharmacol. Biochem. Behav. *52*, 297–303.

Schmitzer-Torbert, N., Jackson, J., Henze, D., Harris, K., and Redish, A.D. (2005). Quantitative measures of cluster quality for use in extracellular recordings. Neuroscience *131*, 1–11.

Seidenbecher, T., Laxmi, T.R., and Pape, H.-C. (2003). Amygdalar and Hippocampal Theta Rhythm Synchronization During Fear Memory Retrieval. *301*, 846–850.

Shah, A.A., and Treit, D. (2003). Excitotoxic lesions of the medial prefrontal cortex attenuate fear responses in the elevated-plus maze, social interaction and shock probe burying tests. Brain Res. *969*, 183–194.

Siapas, A.G., Lubenov, E.V., and Wilson, M.A. (2005). Prefrontal phase locking to hippocampal theta oscillations. Neuron *46*, 141–151.

Sierra-Mercado, D., Padilla-Coreano, N., and Quirk, G.J. (2011). Dissociable roles of prelimbic and infralimbic cortices, ventral hippocampus, and basolateral amygdala in the expression and extinction of conditioned fear. Neuropsychopharmacology *36*, 529–538.

Sotres-Bayon, F., Sierra-Mercado, D., Pardilla-Delgado, E., and Quirk, G.J. (2012). Gating of fear in prelimbic cortex by hippocampal and amygdala inputs. Neuron *76*, 804–812.

Spellman, T., Rigotti, M., Ahmari, S.E., Fusi, S., Gogos, J.A., and Gordon, J.A. (2015). Hippocampal-prefrontal input supports spatial encoding in working memory. Nature *522*, 309–314.

Sterpenich, V., Schwartz, S., Maquet, P., and Desseilles, M. (2014). Ability to maintain internal arousal and motivation modulates brain responses to emotions. PLoS ONE *9*, e112999.

Stujenske, J.M., Likhtik, E., Topiwala, M.A., and Gordon, J.A. (2014). Fear and safety engage competing patterns of theta-gamma coupling in the basolateral amygdala. Neuron *83*, 919–933.

Tort, A.B.L., Komorowski, R.W., Manns, J.R., Kopell, N.J., and Eichenbaum, H. (2009). Theta-gamma coupling increases during the learning of item-context associations. Proc. Natl. Acad. Sci. USA *106*, 20942–20947.

Tye, K.M., Prakash, R., Kim, S.-Y., Fenno, L.E., Grosenick, L., Zarabi, H., Thompson, K.R., Gradinaru, V., Ramakrishnan, C., and Deisseroth, K. (2011). Amygdala circuitry mediating reversible and bidirectional control of anxiety. Nature *471*, 358–362.

Vinck, M., van Wingerden, M., Womelsdorf, T., Fries, P., and Pennartz, C.M.A. (2010). The pairwise phase consistency: a bias-free measure of rhythmic neuronal synchronization. Neuroimage *51*, 112–122.

Neuron, Volume *89*

Supplemental Information

Direct Ventral Hippocampal-Prefrontal Input Is Required for Anxiety-Related Neural Activity and Behavior

Nancy Padilla-Coreano, Scott S. Bolkan, Georgia M. Pierce, Dakota R. Blackman, William D. Hardin, Alvaro L. Garcia-Garcia, Timothy J. Spellman, and Joshua A. Gordon

Figure S1

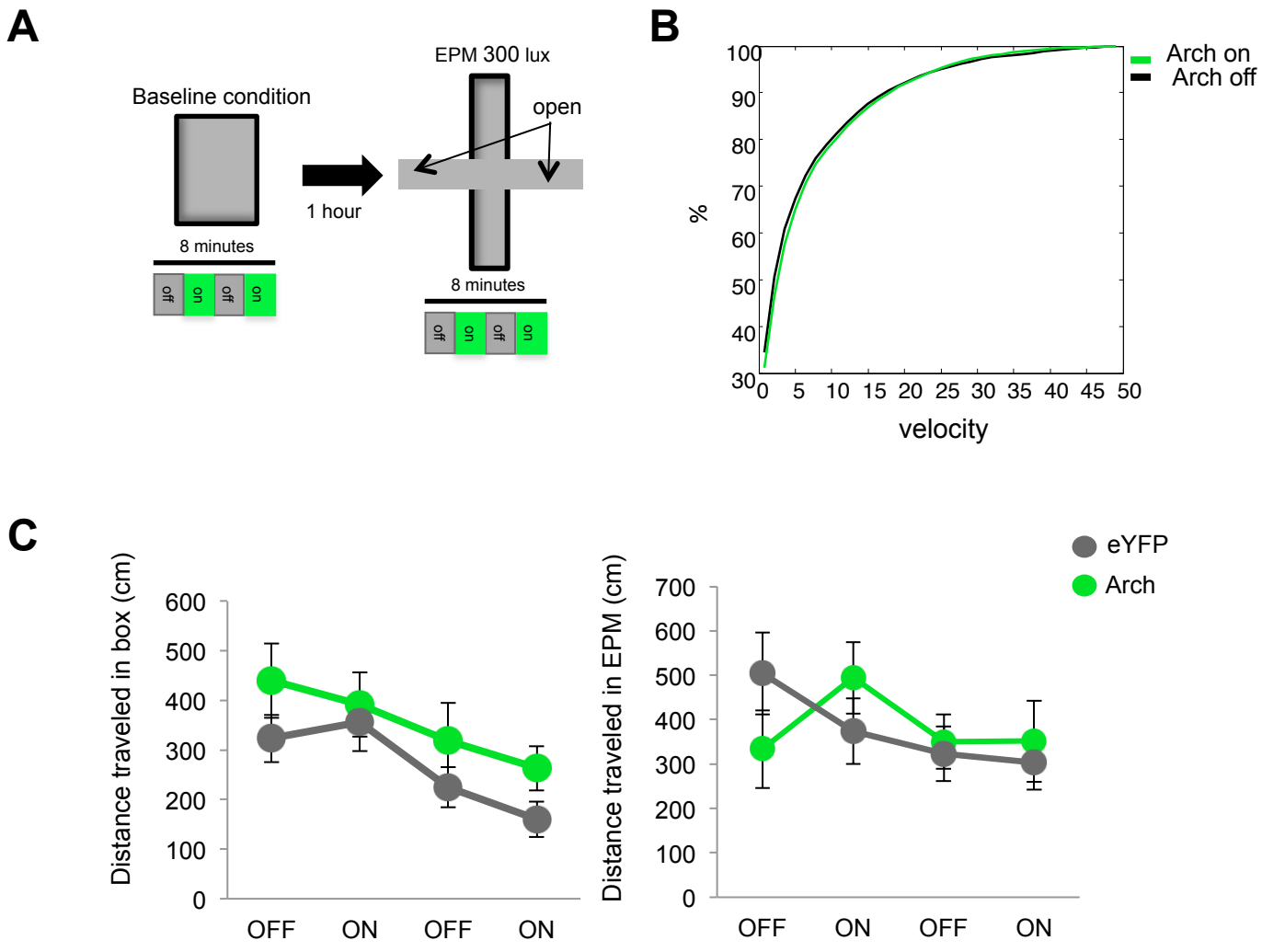

Figure S1, related to Figure 1 : **Inhibition of vHPC input to the mPFC does not affect locomotion.** (**A**) Diagram of behavioral protocol. Locomotion was measured in both a familiar box (left) and the elevated plus maze (right), with 8 minutes of exposure to each. Laser illumination of bilateral vHPC terminals in the mPFC was delivered in two minute epochs, alternating with no illumination. **(B)** Cumulative histograms of average velocity during bilateral terminal inhibition for Arch expressing mice (n=9). **(C**) Effects of terminal inhibition on distance traveled in the baseline box (left), and in the EPM (right) in Arch- and eYFP-expressing mice (n=10 and n=9, respectively). Data are presented as mean +/– SEM throughout, except where otherwise noted.

Figure S2

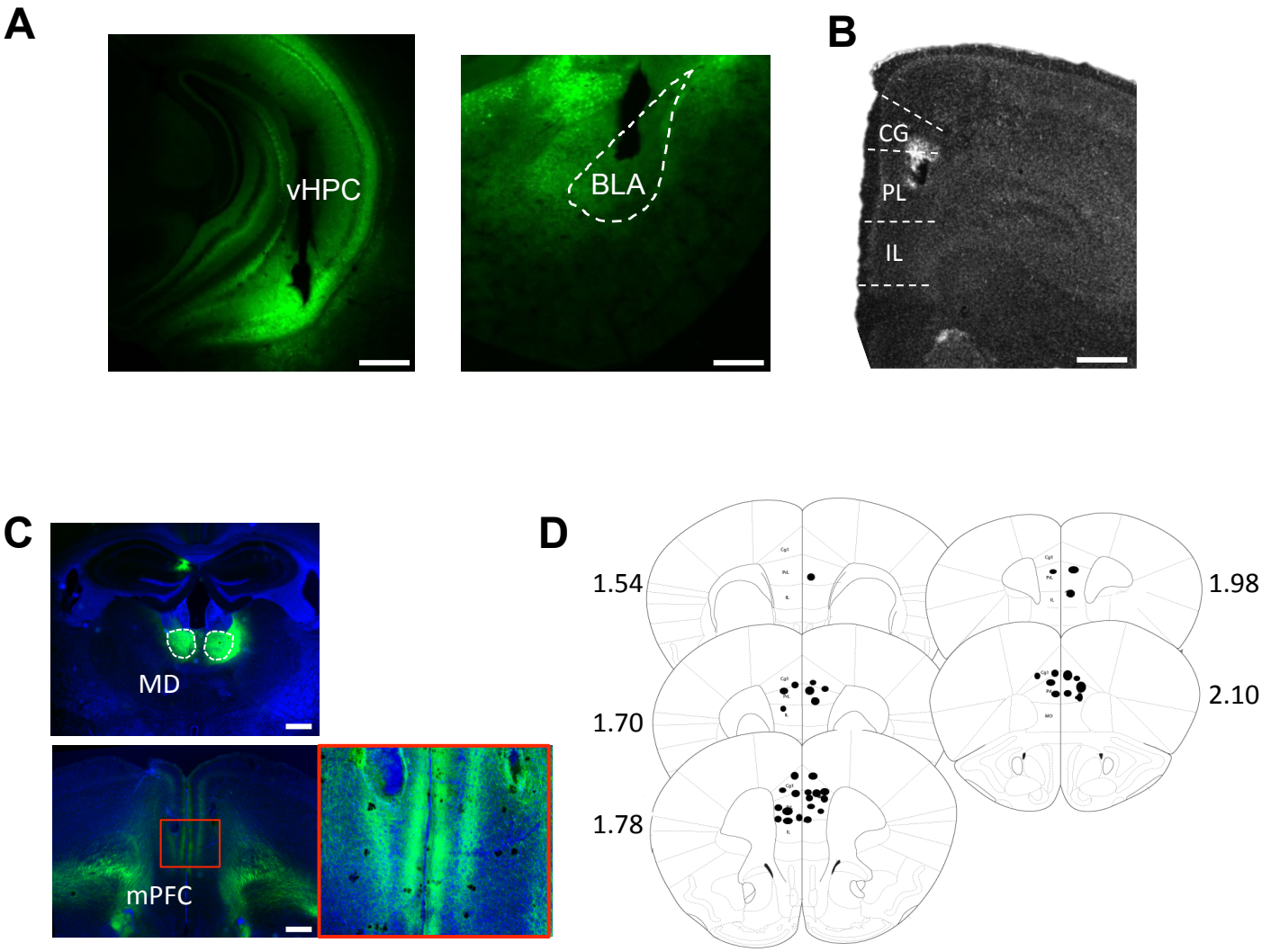

Figure S2, related to Figure 1: **Virally-mediated expression and electrode placement.** (**A**) Representative electrode locations for LFP wires implanted in the vHPC (left) and BLA (right). Green color is eYFP flourescence. White scale bar is 500 um for mPFC and vHPC and 100 um for BLA (**B**) Representative stereo-optrode location in the mPFC, imaged with DAPI (CG: cingulate cortex, PL: prelimbic cortex, IL: infralimbic cortex). (**C**) eYFP-tagged Arch flourescence in cells in the mediodorsal thalamus (MD, top) and terminals in the mPFC (bottom), after MD viral infection. Red square in bottom left indicates region shown magnified in bottom right. White scale bar is 0.5 mm. (**D**) Electrode placements in the mPFC, mostly located in the prelimbic (PL) cortex.

Figure S3

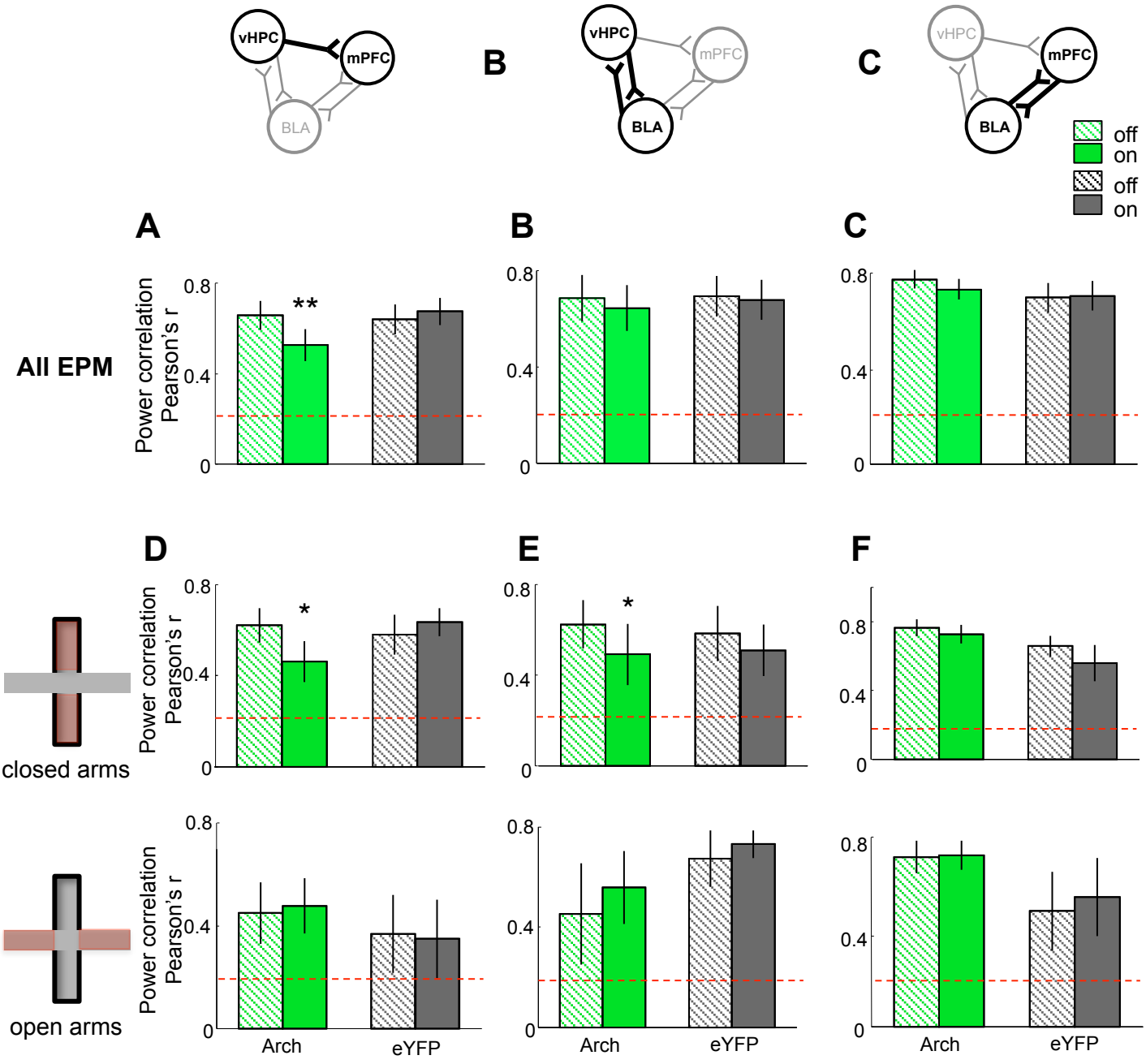

Figure S3, related to Figure 2: Inhibition of hippocampal-prefrontal input disrupts theta power correlation in a pathway-specific manner (**A-C**) Theta power correlations for vHPC-mPFC (**A**) (Arch n=10; eYFP n=11; **, $p < 0.01$ Wilcoxon sign-rank test); vHPC-BLA (**B**) (n=7 per group); and mPFC-BLA (**C**) (Arch n=7; eYFP n=6). (**D-F**) Theta power correlation calculated separately for data from the closed arms (top) and open arms (bottom) for the vHPC-mPFC (**D**) (*, p=0.0234, sign-rank); vHPC-BLA (**E**) (*, p=0.0413, sign rank) and the mPFC-BLA (**F**). Dashed red lines indicate critical value ($p<0.05$) for power correlations generated with shuffled data.

Figure S4

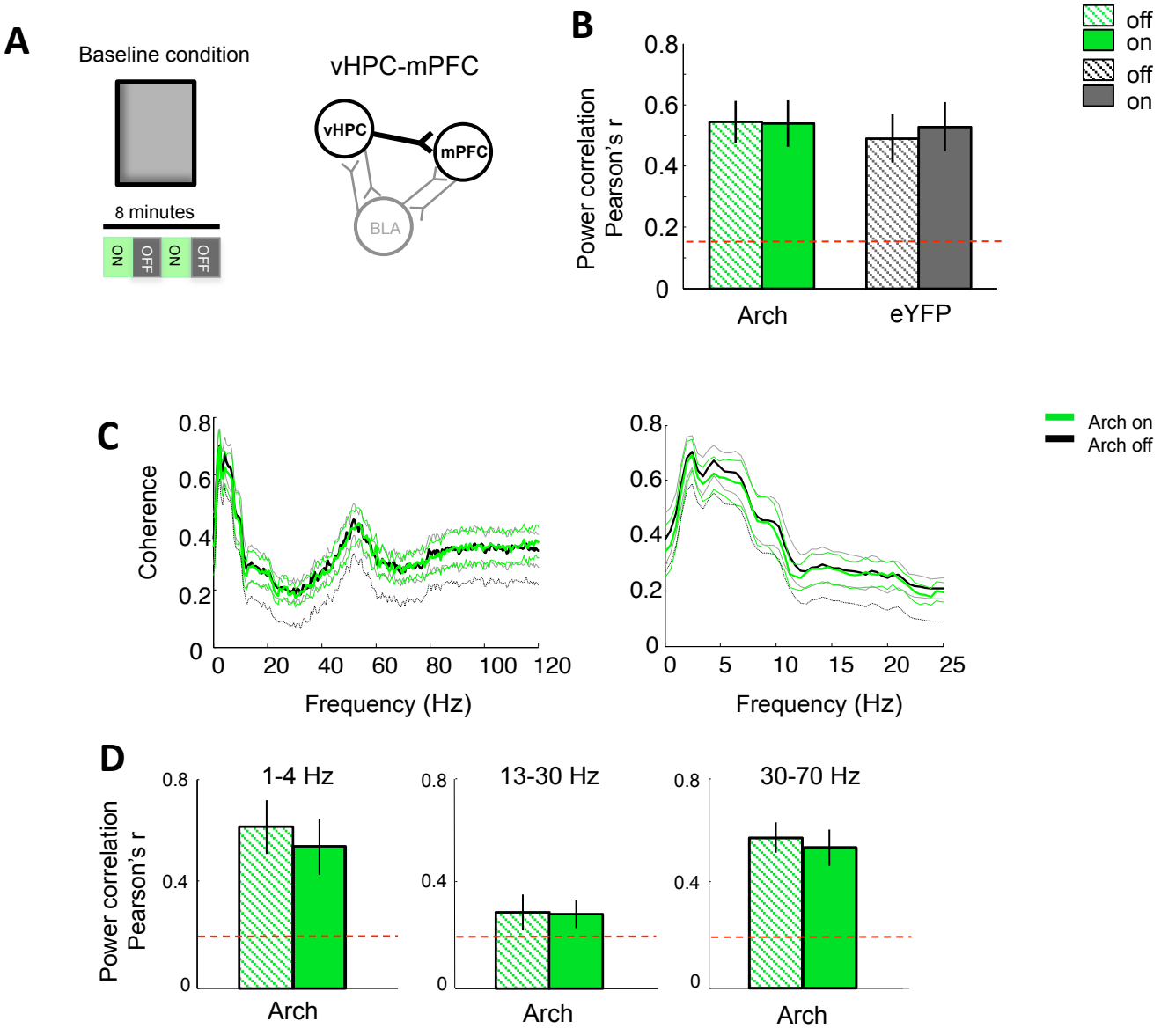

Figure S4, related to Figure 2: Inhibition of vHPC-mPFC pathway disrupts power synchrony in a task and frequency dependent manner (**A**) schematic of the behavioral experiment and the recorded sites. (**B**) Power correlation in the 4-12 Hz range for vHPC and mPFC in the baseline condition (n=10 for arch and n=11 for eYFP). (**C**) Coherence spectral between the vHPC and mPFC in the Arch group during the EPM (mean ± sem). Dashed lines 95% confidence interval. (**D**) Power correlations for vHPC and mPFC LFPs in the delta (1-4 Hz; Wilcoxon sign rank test p=0.13), beta (13-20 Hz) and slow gamma (30-70 Hz) frequency ranges during the EPM. Red lines in **B** and **D** indicate critical value ($p<0.05$) for power correlations generated with shuffled data.

Figure S5

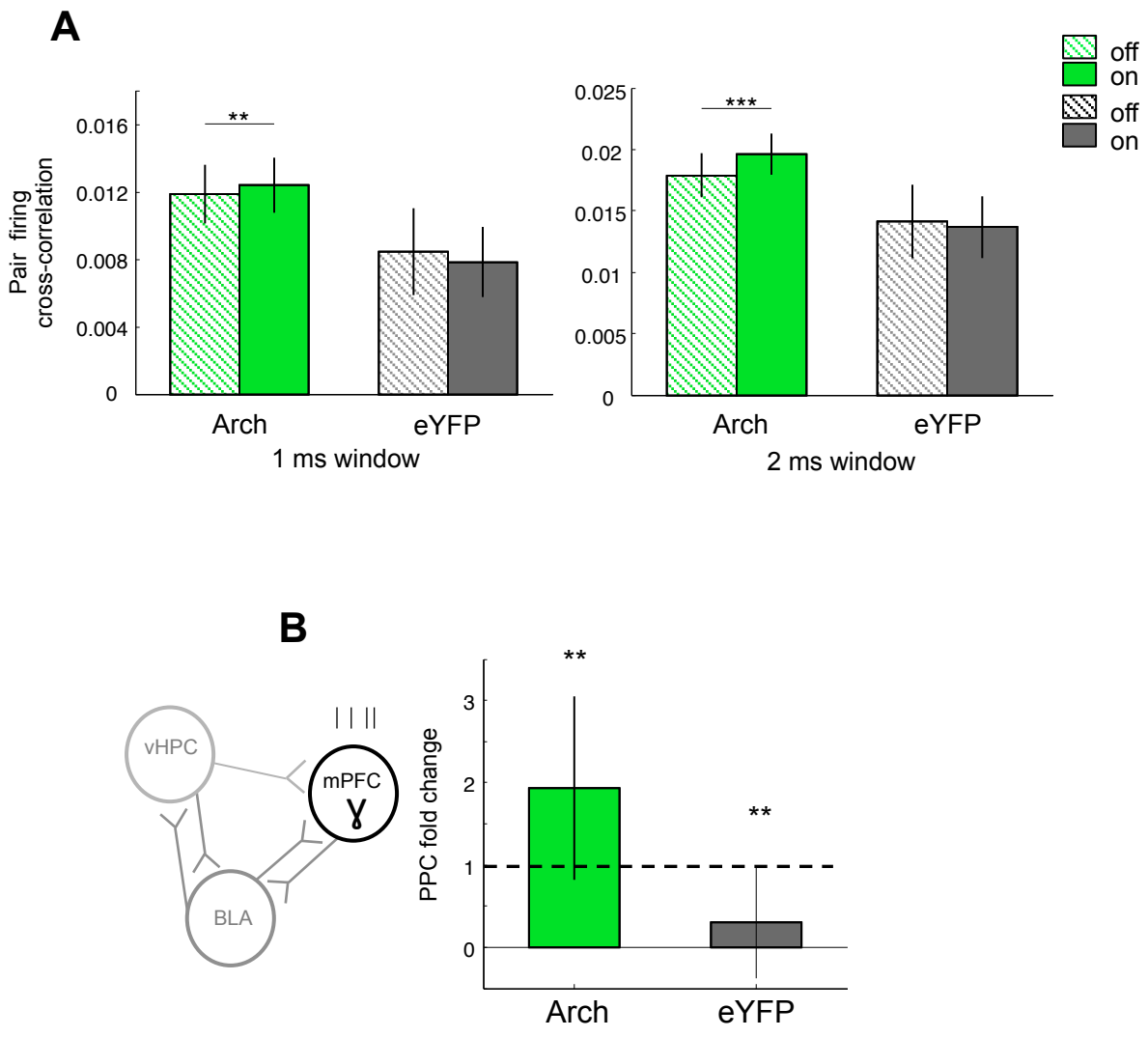

Figure S5, related to Figure 2: Inhibition of vHPC-mPFC pathway increases synchrony within the mPFC. (A) Cross-correlation of spikes during 1 ms window for simultaneously recorded pairs of mPFC single units during the EPM (Arch n=842 ***, p<0.01; eYFP n=416; p=0.26; Wilcoxon paired test). Cross-correlation of spikes during 2 ms window for mPFC simultaneously recorded single units during the EPM (Arch n=842, ***p<0.001; eYFP n=416 p=0.10; Wilcoxon paired test). **(B)** Fold change (ON/OFF) for phase locking strength to local fast gamma (Arch n=79 p<0.01; eYFP n=46 p<0.01; Wilcoxon one sample test). Dashed line is unity (no change).

Figure S6

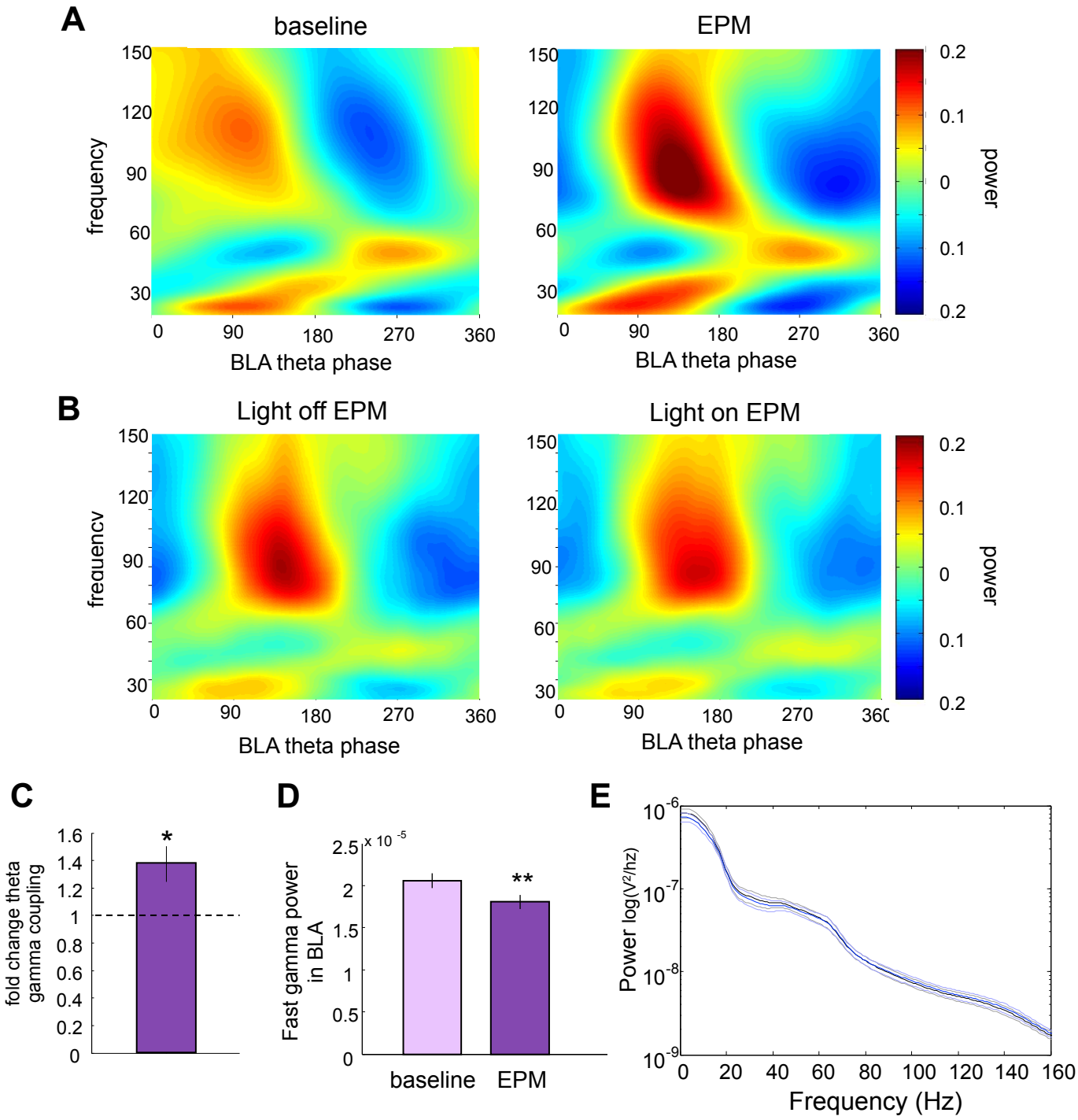

Figure S6, related to Figure 7: The EPM induces alterations in theta-gamma coupling and gamma power. (A) Example BLA comodulogram from the same electrode in the baseline condition (left) and in the EPM (right). **(B)** Averaged comodulograms for Arch animals in the closed arms of the EPM with the light off and the light on. (**C**) Fold change in theta-gamma coupling during the EPM vs baseline, as measured with MRL (n=19; *p<0.05; one sample Wilcoxon sign rank test). (**D**) Average fast famma power in the BLA during the baseline recording and the EPM (n=19, **p<0.01; paired Wilcoxon sign rank test). (**E**) Averaged BLA power spectra in the closed arms of the EPM for Arch injected animals (light off=black; light on=blue).

Figure S7

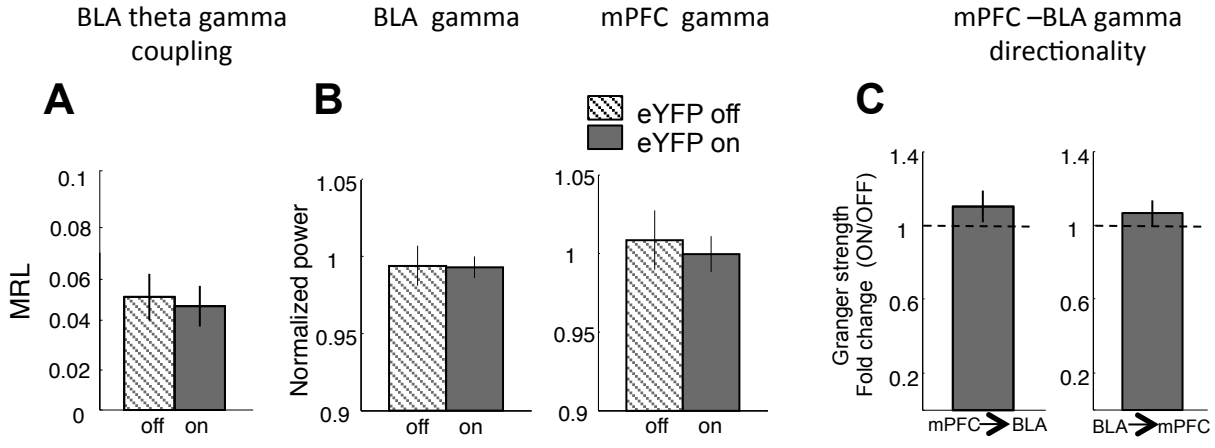

Figure S7, related to Figure 7: Illumination does not affect BLA or mPFC fast gamma measurements in eYFP animals. (A) BLA theta and fast gamma (70-120 Hz) coupling (n=9, p=0.25 Wilcoxon sign rank paired test). **(B)** Fast gamma power in BLA (p=0.36; Wilcoxon sign rank paired test) and mPFC (eYFP n=11, p=0.59) **(C)** Fold change in granger directionality strength in the mPFC to BLA direction (left) and the BLA to mPFC direction (right). Dashed lines indicate unity (no change).